Full text open access online (Since 2001)

PRINT: ISSN 0972-3757 ONLINE: ISSN 2456-6330
Int J Hum Genet, 25(3): 132-150 (2025)
DOI: 10.31901/24566330.2025/25.03.918

Construction and Analysis of a Uterine Corpus Endometrial Carcinoma Prognostic Model Based on Disulfidoptosis-Related lncRNAs

Jindong Miao, Kaili Wang, Mengcheng Cai, Wen Cheng, Chaoqin Yu*, Danying Zhang* and Ruipin Yao

[a]Department of Traditional Chinese Gynecology, The First Affiliated Hospital of Naval Medical University, Shanghai, 200433, China

KEYWORDS Disulfidoptosis. Immune Infiltration. Long Non-coding RNA. Prognostic Markers. Uterine Corpus Endometrial Carcinoma

ABSTRACT Disulfidoptosis, an emerging programmed cell death modality form, is linked to long non-coding RNAs (lncRNAs). This study aimed to develop a disulfidoptosis-related lncRNA (drlncRNA) predictive algorithm for endometrial carcinoma of uterine corpus (UCEC) and explore its association regarding overall survival (OS) and the tumour immune microenvironment (TME). Molecular profiling and patient-derived clinical information of UCEC individuals diagnosed in The Cancer Genome Atlas (TCGA) were analysed. Linear correlation coefficient identified drlncRNAs, and Cox and LASSO regression established a 4-drlncRNA prognostic model. Patients were grouped by risk score, with high-risk groups showing shorter OS. The model independently predicted OS, and high-risk patients had higher tumour mutation burden (TMB) and altered immune infiltration within tumour tissues. This drlncRNA model effectively predicts UCEC prognosis, aiding personalised treatment.

INTRODUCTION

Corpus uteri Uterine endometrial carcinoma (UCEC) is ranked within the most prevalent gynaecologic malignancy malignancies affecting women globally reproductive system, typically occurring in postmenopausal women. According to global cancer statistics, UCEC ranks fourth in incidence among female malignancies, following breast, lung, and colorectal cancers. In 2022, an estimated 65,950 new UCEC cases were diagnosed within the United States, representing approximately 7 percent among the total female incident malignancies. Projected incidence of UCEC-related deaths is 12,550, representing about 4 percent of female mortality from malignancies within the United States (Siegel et al. 2022).

Current therapeutic interventions for malignancies encompass surgical resection, radiation treatment, cytotoxic drug regimens, and hormonal modulation therapy, with specific plans tailored to individual patient conditions (Wang et al. 2022). Surgical resection is preferred for early-stage endometrial cancer, while advanced cases often require concurrent chemoradiation therapy (Koskas et al. 2021). Recently, novel treatments like immunotherapy and targeted therapy have been developed and are under continuous study and application (Gordhandas et al. 2023; Hecking et al. 2022; Mutlu et al. 2022). Nevertheless, challenges remain, especially for high-grade endometrial cancer, which tends to recur and is prone to advanced or metastatic disease (Wang et al. 2022). Advanced-stage diagnoses frequently occur in patients presenting with non-specific clinical manifestations, leading to difficult treatments and poor prognosis. Current treatments have limitations, including side effects of endocrine therapy and immunotherapy (Kulkarni et al. 2020; Murray et al. 2019; Patel et al. 2021), and issues like chemotherapy resistance (Alhaj-Suliman et al. 2023), necessitating further exploration of new treatment methods and strategies.

With advances in biotechnology and data analysis, genomic data are increasingly used to study the pathogenesis and treatment strategies of endometrial cancer (Karpel et al. 2023). Recent studies highlight the significant functional influence of long noncoding RNAs (lncRNAs) (lncRNAs) in tumorigenesis endometrial malignant neoplasm, identifying it as a potential prognostic marker. LncRNA prognostic models related to regulated cellular necrosis, including programmed necrosis (Lin et al. 2023), ferroptosis (Qin et al. 2023), cuproptosis (Chen et al. 2022b), and pyroptosis (Liu et al. 2022), have become research hotspots. Recently, Liu et al. (2023) discovered a new manifestation of regu-

lated cellular demise, termed disulfideptosis. Under glucose deprivation starvation, cells with high SLC7A11 manifestation accumulate intracellular disulfides like cystine, inducing disulfide stress that increases disulfide bonds in the actin cytoskeleton, causing actin filament contraction, cytoskeletal destruction, and cell death. Thus, this scientific examination aims at a predictive framework of lncRNA associated with disulfideptosis (drlncRNA) to predict OS in UCEC and propose new treatment strategies.

Objectives

This investigation seeks to delineate disulfideptosis-related long noncoding RNA transcripts (drlncRNAs) in uterine corpus endometrial carcinoma (UCEC), construct a drlncRNA-based prognostic framework for forecasting overall survival, and examine its correlation in the context of the tumour immune milieu and sensitivity to anticancer drugs.

METHODOLOGY

Public Data Collection

Data from UCEC patients were accessed through the genomic information Repository (GDC) dataset interface (https://portal.gdc.cancer.gov/repository). Ribonucleic acid sequencing (RNA-sequencing (seq) datasets (seq)) data were collected employing the fragments per kilobase million (FPKM) normalisation method platform and normalised through logarithmic transformation. Specimens lacking comprehensive clinical data were excluded to avoid statistical bias. A total of 544 patients, comprising 554 neoplastic tissue specimens and 23 healthy controls tissue samples, were included. These participants were stratified for partitioning into training versus validation subsets at a 1:1 allocation proportion.

Identification of Differentially Expressed Disulfideptosis-related LncRNAs

A panel of ten disulfideptosis-related geneslinked the following ten genes, namely, GYS1, LRPPRC, NCKAP1, NDUFA11, NDUFS1, NUBPL, OXSM, RPN1, SLC3A2 and SLC7A11, identified from previous research. Their transcriptional abundance in malignant and non-malignant specimens were analysed via DESeq2 algorithm with univariate Cox proportional hazards modelling ($p < 0.05$). Survival-associated value was assessed by integrating these genes with immunohistochemical data via the Human Protein Atlas database resource (HPA; https://www.proteinatlas.org/). Pearson association study identified disulfideptosis-associated lncRNAs (drlncRNA) using a filter condition with Pearson correlation coefficients exceeding 0.3 ($p<0.001$). The Wilcoxon test and threshold parameters for $|\log2FC|\geq1$ and p.adj.<0.05 selected tumour-normal specific lncRNAs with differential expression patterns. Overlapping the selected lncRNAs determined DE-drlncRNAs, and a risk forest diagram was created.

Establishment and Evaluation of drlncRNA Prognostic Model

Matching the expression of DE-drlncRNAs with survival rates, prognostic lncRNAs were pinpointed via univariate Cox proportional hazards modelling in DE-drlncRNAs ($P<0.05$). Penalised Cox modelling via 'survival' and 'glmnet', screened for the best prognostic-related DE-drlncRNAs. Using multivariate Cox proportional hazards modelling, the researchers developed a drlncRNA prognostic index. Patient-specific risk scores were computed via the established equation. Risk Score = (Expression of AC139795.2 × 0.516042024432212) + (Expression of Z69733.1 × 0.607799707479734) + (Expression of EMSLR × 0.609578526049159) + (Expression of AC020765.2 × (-0.545526642504592)).

The coefi represents the regression coefficient, while exp denotes the lncRNA expression values after normalisation. The median cutoff classified UCEC stratified subjects into distinct prognostic categories. The "survival" R package executed Kaplan-Meier survival analysis (KM). Kaplan-Meier evaluation across training, validation, and complete cohorts set to compare OS of the groups. ROC curve analysis evaluation via the 'pROC' and 'Hmisc' packages, evaluated the model's predictive precision, measured by the area under the curve (AUC). The chi-square validation evaluated the correlation pertaining to the prognostic risk stratification system and clinical pathological pathological characteristics. Cox regression analysis (univariable and multivariable) assessed the risk score's independent prognostic significance.

Construction and Evaluation of the Nomogram

The researchers developed a prognostic prediction model via the 'rms' package alongside the 'survival' R package to forecast the prognostic index and clinical outcomes pathological attributes of UCEC subjects. Calibration curves and time-related ROC curve analyses evaluated the nomogram's effectiveness.

Functional Enrichment Analysis

Molecular function classification (GO) and pathway enrichment analysis (KEGG) pathway functional overrepresentation, utilising the "clusterProfiler" R software toolkit, identified enriched pathways of risk differential genes. Results were presented in a bar chart, showing enriched pathways in biological processes, cellular components, and molecular functions, as defined by the Gene Ontology (GO) consortium. These screening criteria existed as logFC filter = 0.05 and fdr = 0.05. GSEA toolkit (v4.3.2; http://www.gsea-msigdb.org/gsea/index.jsp) analysed potential enriched pathways between groups. A p.adj. <0.05 and a modelled estimate of 1000 reached statistical significance.

Analysis of Tumour Mutational Burden (TMB) and Immune Cell Infiltration Levels

Tumour-specific genetic alteration profiles of UCEC patients from TCGA were evaluated with the 'maftools' R package to investigate TMB differences among groups. K-M survival analysis divided subjects into low and high TMB stratification using median-derived cutoffs value. Linear correlation assessment via Pearson's method determined the association of prognostic score and TMB. The CIBERSORT algorithm evaluated leukocyte population levels, and tumour immune dysfunction and exclusion (TIDE) framework resource (http://tide.dfci.harvard. edu/) assessed immunological evasion propensity across prognostic strata.

Drug Sensitivity Evaluation

The 'pRRophetic' computational toolkit predicted half-maximal inhibitory concentrations of common antineoplastic agents from the Genomics of Drug Sensitivity in Cancer (GDSC) database (https://www.cancerrxgene.org/) to assess pharmacological responsiveness differences across prognostic strata.

Statistical Analysis

Statistical significance was set at $P<0.05$ unless specified in other cases stated. Statistical computations were conducted using R 4.1.3. Pearson correlation analysis calculated correlation coefficients, with log-rank statistics determined KM survival plot statistical significance. The "heatmap" R package created a heatmap. Cox proportional hazards modeling with univariate and multivariable adjustments, using SPSS version 25, identified independent prognostic factors. Statistical visualisation was performed using GraphPad Prism v9.0 to produce forest diagrams.

RESULTS

Differentially Expressed Disulfideptosis-related Genes in UCEC

The study flowchart is presented in Figure 1. The researchers analysed ten disulfide stress-associated genetic factors in 554 UCEC samples and 23 normal tissue samples. The analysis revealed that 6 genes (GYS1, NCKAP1, NDUFA11, NUBPL, OXSM and RPN1) that showed significant differential expression, while LRPPRC, NDUFS1, SLC3A2, and SLC7A11 did not show significant differences between UCEC and normal tissue samples (Fig. 2A-J: Fig. 2A for GYS1, Fig. 2B for LRPPRC, Fig. 2C for NCKAP1, Fig. 2D for NDUFA11, Fig. 2E for NDUFS1, Fig. 2F for NUBPL, Fig. 2G for OXSM, Fig. 2H for RPN1, Fig. 2I for SLC3A2, Fig. 2J for SLC7A11). Kaplan-Meier (KM) curve analysis indicated that abnormal expression of LRPPRC (Fig. 2L), NDUFA11 (Fig. 2N), and OXSM (Fig. 2Q) exhibited a correlation with overall survival (OS) in the TCGA-UCEC dataset ($P<0.05$), whereas the expression of GYS1 (Fig. 2K), NCKAP1 (Fig. 2M), NDUFS1 (Fig. 2O), NUBPL (Fig. 2P), RPN1 (Fig. 2R), SLC3A2 (Fig. 2S), and SLC7A11 (Fig. 2T) showed no significant association with OS. Protein abundance protein expression data from the Human Protein Atlas (HPA) resource were served to examine OXSM (Fig. 2U, V) and LRPPRC (Fig. 2W, X) in UCEC tissues compared to normal tissues. However, no immunohistochemical data for NDUFA11 in UCEC tissues were available in the HPA database. The

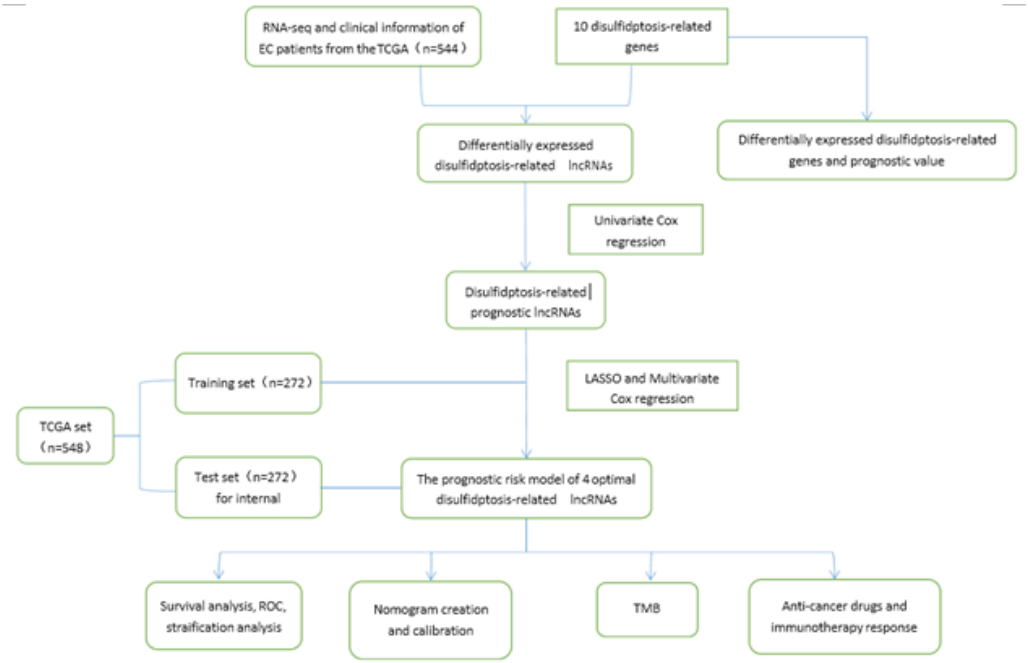

Fig. 1. Flowchart of this study

evidence indicates disulfideptosis contributes to pathogenic processes and prognosis of UCEC.

Establishment of the drlncRNA Signature Prognostic Model

Using criteria with log2-transformed fold changes exceeding 1 in absolute value and FDR-controlled p-values below 0.01, the researchers identified 16,876 TCGA-identified differentially expressed long noncoding RNAs (lncRNAs). Pearson's product-moment correlation revealed 525 disulfideptosis-associated long noncoding RNAs (lncRNAs). A Sankey diagram further visualized the correlation between disulfideptosis-related genes and all 660 drlncRNAs identified in the initial screening (Fig. 3D). The complete cohort was stratified into random subsets UCEC TCGA-enrolled patients into a training set and a validation settesting group and conducted LASSO-regularised Cox proportional hazards modelling in the training cohort. This analysis additionally screened out the 12 best DE-drlncRNAs related to prognosis, of which three were protective factors and nine were risk factors (Fig. 3B, C). The 12 optimal prognostic-related DE-drlncRNAs are explicitly listed in Fig. 3A, and a shock plot was used to illustrate their correlation with disulfideptosis-related genes (Fig. 3E). A survival prediction model composed of four long noncoding RNA (lncRNA) signatures were developed through multivariable proportional hazards model proportional hazards modelling (Fig. 3F). Patient-specific risk scores were computed via the designated algorithm:

Risk Score=AC139795.2×(0.516042024432212)+Z69733.1×(0.607799707479734)+EMSLR×(0.609578526049159)+AC020765.2×(-0.545526642504592).

The clinicopathological features of the UCEC subjects within both the model development and validation sets were shown in Table 1.

Evaluation and Validation of drlncRNA Prognostic Risk Models

The heatmap showed that AC139795.2, Z69733.1, and EMSLR were hazard factors, while AC020765.2 was a protective factor for UCEC prognosis. The Kaplan-Meier analyses demonstrated markedly inferior outcomes among patients stratified to the elevated-risk group patient subgroup shorter versus the low-risk group

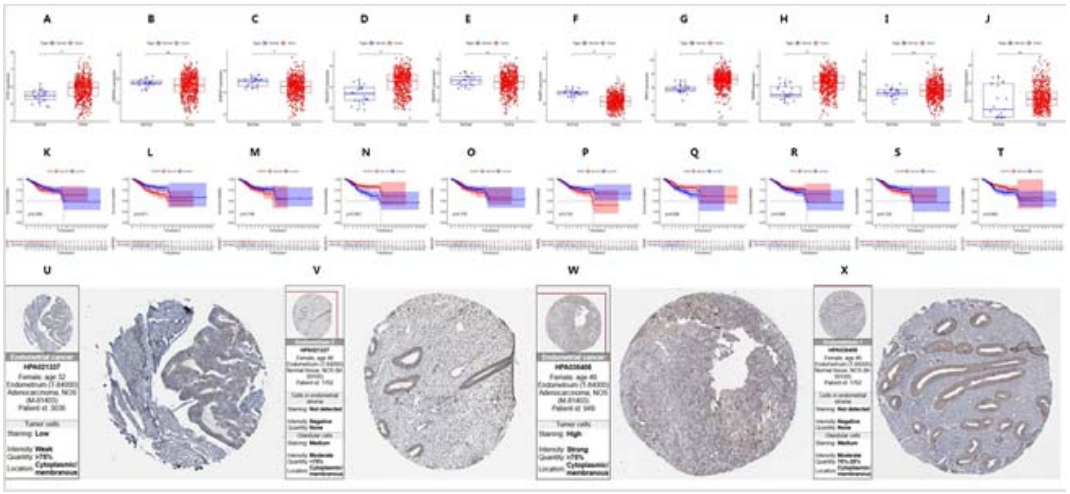

Fig. 2. Correlation between disulfideptosis-related genes and prognosis of endometrial cancer
A-J: Expression differences of 10 disulfideptosis-related genes in normal tissues and endometrial cancer tissues
K-T: Correlation between high and low expression of the 10 disulfideptosis-related genes in endometrial cancer tissues and OS prognosis of endometrial cancer
U, V: OXSM immunohistochemical smears of endometrial cancer tissue and normal tissue
W, X: LRPPRC immunohistochemical smears of endometrial cancer tissue and normal tissue

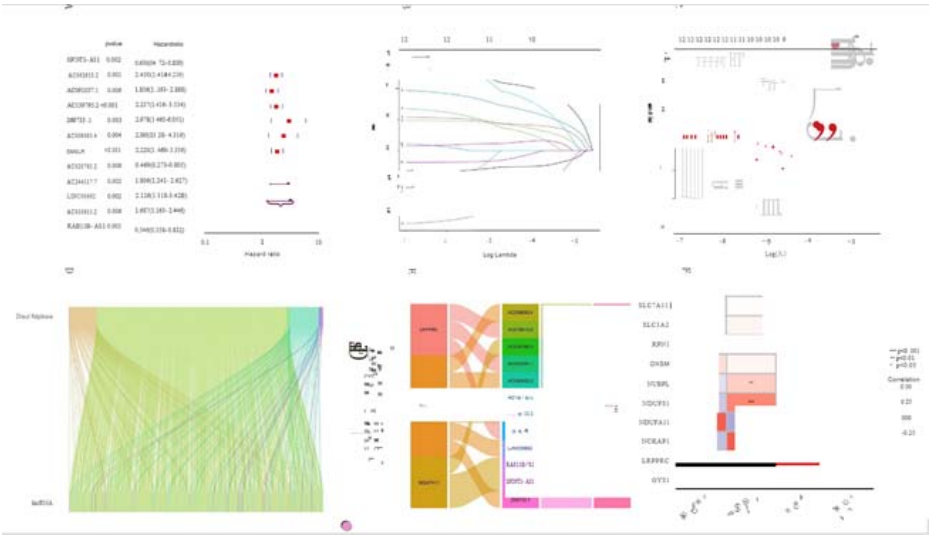

Fig. 3. Establishment of the drlncRNA signature prognostic model
A: 12 best prognostic-related DE-drlncRNAs
B: LASSO coefficients of the 12 best prognostic-related DE-drlncRNAs
C: 10-fold cross-validation for variable selection in the LASSO algorithm.
D: Sankey diagram showing the correlation between disulfideptosis-related genes and all 660 drlncRNAs
E: Shock plot showing the correlation of disulfideptosis-related genes with the 12 best prognostic-related DE-drlncRNAs
F: Regulatory relationship between the four drlncRNAs involved in the prognosis model and disulfideptosis-related genes

Table 1: The clinical and pathological characteristics of the UCEC patients in both the training and testing sets

Covariates	*Type*	*Total(n=544)*	*Test(n=272)*	*Train(n=272)*	*P value*
Age	<=65	307 (56.43%)	149 (54.78%)	158 (58.09%)	0.4286
Age	>65	235 (43.2%)	123 (45.22%)	112 (41.18%)	
Age	Unknown	2 (0.37%)	0 (0%)	2 (0.74%)	
Grade	G1	99 (18.2%)	46 (16.91%)	53 (19.49%)	0.7044
Grade	G2	121 (22.24%)	60 (22.06%)	61 (22.43%)	
Grade	G3	324 (59.56%)	166 (61.03%)	158 (58.09%)	

cohort, accompanied by markedly shorter overall survival (OS), validated during the model development phase, testing, and entire dataset. This was reflected in the risk score distribution of training group (Fig. 4A), test group (Fig. 4B), and all patients (Fig. 4C) showing a clear gradient between high and low risk subgroups; the OS distribution (Fig. 4D: training group, Fig. 4E: test group, Fig. 4F: all patients) corresponded with risk scores, with higher mortality in the high-risk group; the expression levels of the 4 drlncRNAs (Fig. 4G: training group, Fig. 4H: test group, Fig. 4I: all patients) further confirmed the differential expression patterns of hazard and protective factors. Kaplan-Meier survival analysis results (Fig. 4J: training group, Fig. 4K: test group, Fig. 4L: all patients) consistently verified shorter OS in the high-risk group across all cohorts. These findings demonstrate that the prognostic model exhibits reliable predictive accuracy sensitivity and predictive ability regarding overall survival (OS) in UCEC patient cohort.

Kaplan-Meier Survival Analysis of PFS and Principal Component Analysis (PCA) of the drlncRNA Risk Model

To elucidate the clinical relevance and predictive capacity of the drlncRNA signature, Figure 5 was constructed. Figure 5A displays a forest plot from univariate Cox regression, outlining hazard ratios (HRs) of clinical factors (age, tumor stage) in relation to overall survival (OS) in UCEC. Figure 5B presents a multivariate Cox regression forest plot, adjusting for confounders to identify independent prognosticators. Time-dependent receiver operating characteristic (ROC) curves were used to gauge predictive accuracy over time: Figure 5C shows ROC curves for 1-, 3-, and 5-year OS based on the drlncRNA signature, with area under the curve (AUC) values of 0.817, 0.822, and 0.814, respectively; Figure 5D depicts ROC curves for the same time points using a combination of the drlncRNA signature and clinical stage, yielding AUCs of 0.819, 0.818, and 0.819, confirming the model's strong predictive performance. Figure 5E illustrates Kaplan-Meier survival curves comparing OS across groups stratified by the drlncRNA risk score (high-risk vs. low-risk) and clinical stage, revealing notable survival disparities. Figure 5F combines a calibration plot and risk score distribution, with box plots and density curves showing predicted risk distributions across subgroups defined by age, stage, and grade, and dotted lines marking the median risk cutoff. The nomogram calibration curve in Figure 5G evaluates the agreement between nomogram-predicted probabilities (for 1-, 3-, and 5-year OS) and actual observed survival, demonstrating good concordance. Subgroup analyses by tumor grade (G1, G2, G3) were also conducted: Figure 5H shows Kaplan-Meier curves for G1 tumors; Figure 5I for G2 tumors; and Figure 5J for G3 tumors. These results indicate the drlncRNA signature can stratify prognosis within grade subgroups, particularly in G3 tumors where high-risk patients have significantly poorer survival.

The Clinical Significance of Prognostic Models

Multivariate and single-variable Cox regression validated the autonomous prognostic significance pertaining to risk score and histologic grade prognostic variables influencing overall survival (OS) in UCEC patients ($P<0.001$). The forest plots from univariate (Fig. 6A) and multivariate (Fig. 6B) Cox regression illustrate the hazard ratios of risk score, age, and histologic grade, confirming the independent prognostic value of the risk score. The risk score exhibited

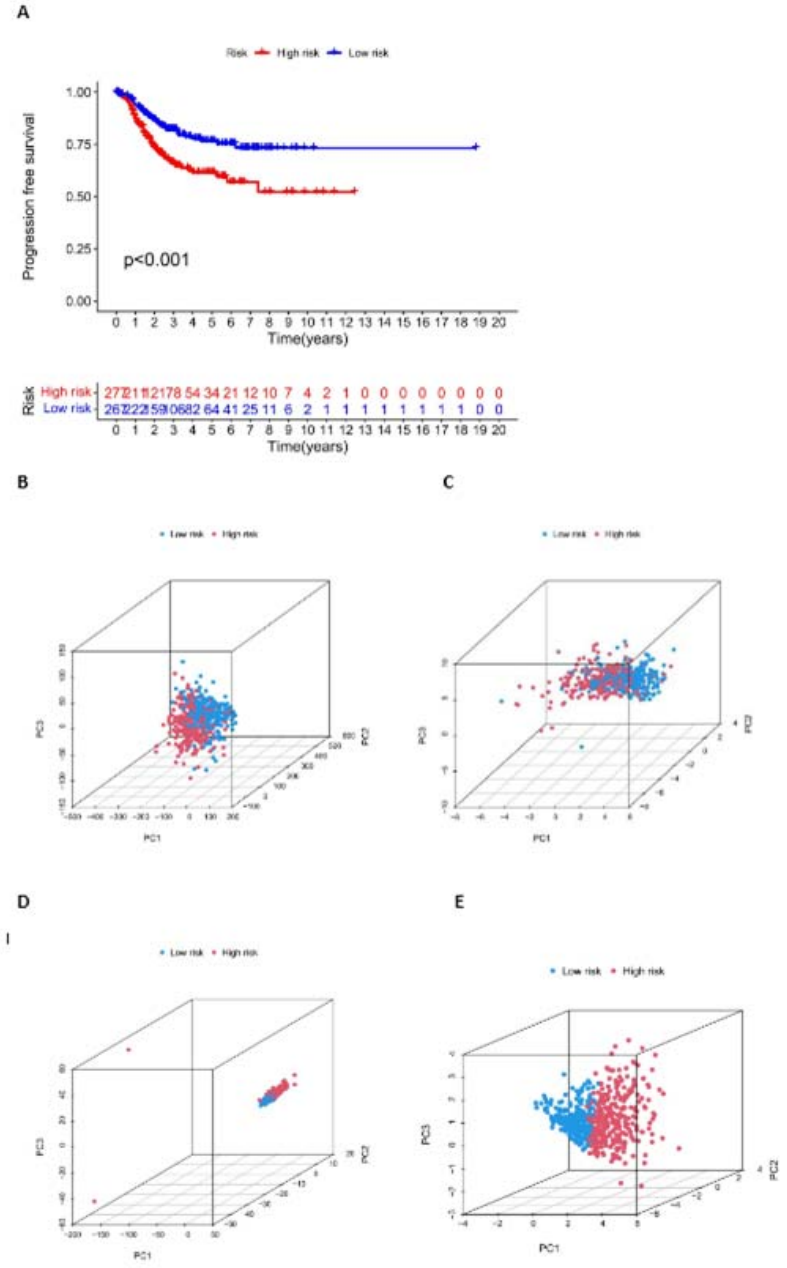

Fig. 4. Prognostic value of the risk model in different ensembles
A-C: Risk score distribution of drlncRNA-based EC patients in the training group, test group, and all patients
D-F: OS distribution in the training group, test group, and all patients.
G-I: The expression levels of 4 drlncRNAs in the training group, test group, and all patients
J-L: Kaplan-Meier survival analysis of patient OS in the training group, test group, and all patients

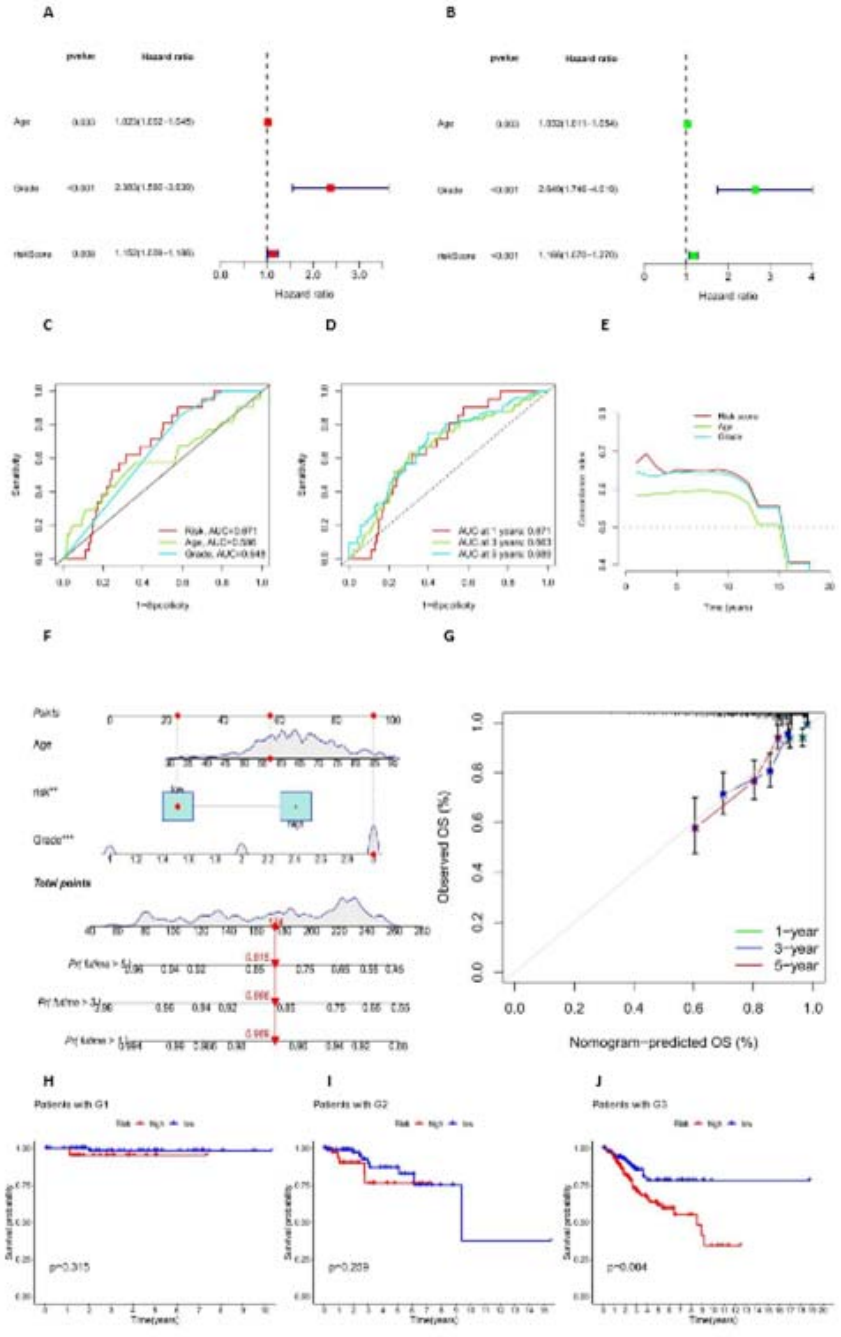

Fig. 5. Kaplan-Meier survival analysis of patient PFS according to the drlncRNA risk model (A) and principal component analysis of the drlncRNA risk model (B-E)

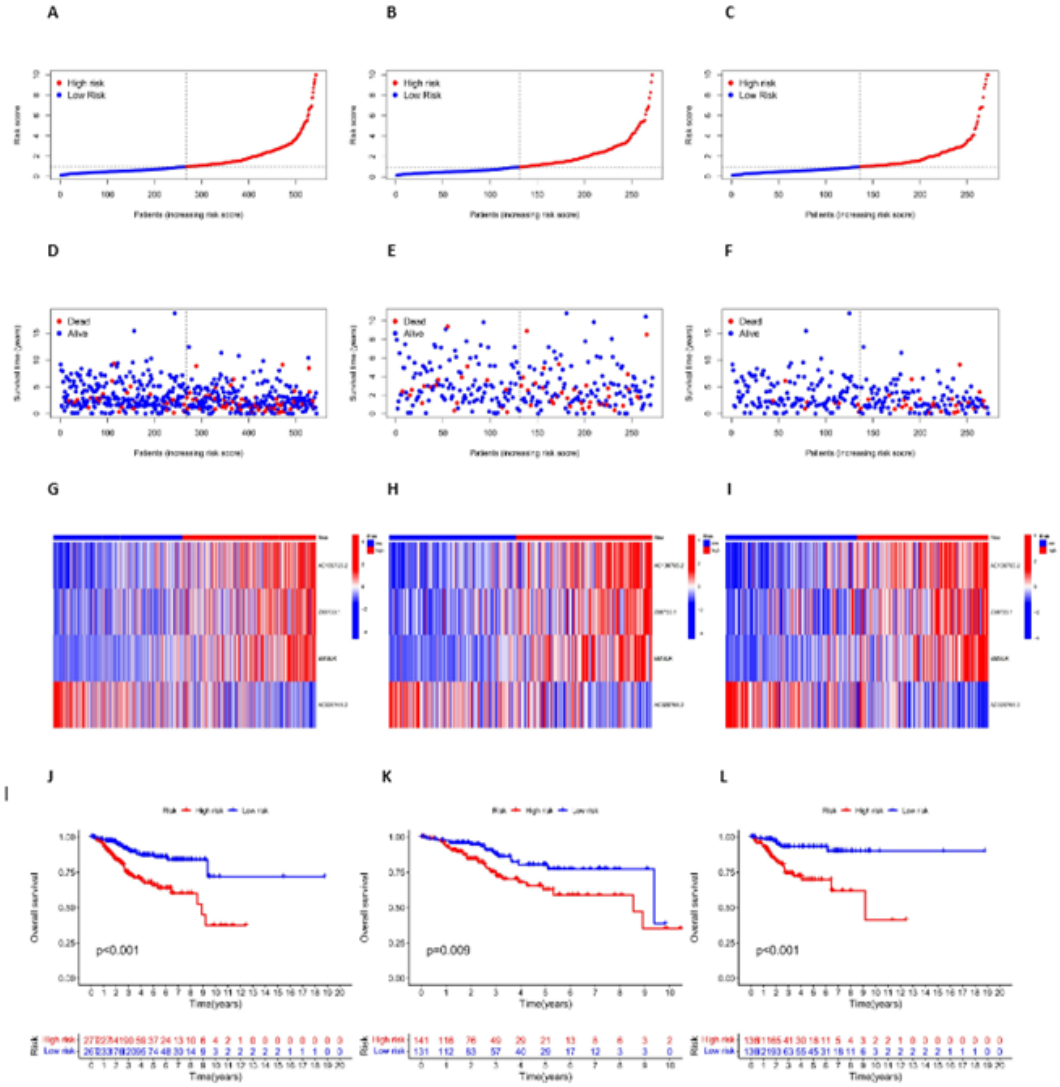

Fig. 6 Validation of the clinical significance of pathological models
A: Multivariate Cox regression analysis
B: Univariate Cox regression analysis
C: Multivariate ROC analysis
D: Based on time-dependent ROC analysis
E: C-index analysis
F: Construction of the nomogram.
G: Calibration curve of the nomogram.
H-J: OS K-M survival analysis of high and low risk groups for patients in pathological grades G1, G2, and G3

better OS prediction performance than age alongside histopathological grading, as indicated through elevated area under the ROC curve (AUC) metrics in multivariate and time-dependent ROC analyses (Fig. 6C, D). The prognostic index also showed good consistency in predicting the OS of UCEC patients, indicated by higher C-index values than age and pathological grade (Fig. 6E). A nomogram combining the risk score with various clinical pathological information predicted the OS of UCEC patients (Fig. 6F), and the calibration curve showed high accuracy in predicting survival rates (Fig. 6G). Stratified analysis of the elevated risk group demonstrated markedly reduced overall survival outcomes within the pathological grade G3 subgroup (P=0.004) (Fig. 6H-J).

Enrichment Analysis of Functions and Pathways

Gene ontology (GO) annotations set enrichment assessment revealed that the gene sets demonstrated significant enrichment within molecular functions such as signal receptor binding receptor-mediated signalling, ligand-binding functionality and microtubule binding. Enrichments were also found in cellular components like the fibrous extracellular matrix with collagen components, antigen-binding immunoglobulin assemblies and synapses between neurons, and in biological processes such as axonogenesis, pattern specification process, synaptic organisation, and localisation (Fig. 7A-D). Pathway-based functional enrichment analysis revealed significant enrichments in KEGG annotated pathways, and the gene sets showed significant enrichment in biological pathways associated with axonogenesis, synaptic organisation, localisation, and pattern specification process (Fig. 7E-G). Gene set enrichment analysis (GSEA) did not show statistically overrepresented signaling cascades within either the elevated-risk group cohort versus the minimal-risk counterpart (Fig. 7H-J).

Analysis of Immune Cell Infiltration and TIDE

The researchers juxtaposed proportions pertaining to 13 immune parameters cell functions and quantified 22 immune cell infiltration patterns across high-risk versus low-risk cohorts. Several immune cell functions, such as II interferon response, immune checkpoints, T lymphocyte activation pathways, T cell suppressive signalling, and pro-inflammatory effects, were more significant among the low-risk group. Conversely, the elevated-risk group subgroup demonstrated higher significance for I interferon response and I major histocompatibility complex (Fig. 8A). Applying the CIBERSORT method, the researchers identified distinct infiltration percentages of immune cells: the elevated-risk group cohort exhibited elevated levels of macrophages, particularly M2-polarised subsets, along featuring elevated levels of activated dendritic cell subsets, while the infiltration rate of plasma cells, CD8+ T cells, immunosuppressive Treg lymphocytes and quiescent dendritic cells was higher among the low-risk group (Fig. 8B). Pearson correlation analysis showed that the infiltration values of M1-polarised macrophages (M1) (Fig. 8G), M2-polarised macrophages (alternative activation) (Fig. 8H), activated dendritic cells (Fig. 8I), and monocytes demonstrated a robust positive association with the risk stratification index ($p<0.05$), whereas plasma cells (Fig. 8C), CD8+ T cells (Fig. 8D), regulatory T cells (Tregs) (Fig. 8E), and quiescent dendritic cells (Fig. 8F) exhibited significant inverse associations (Fig. 8J for integrated correlation analysis). The TIDE database indicated that TIDE potential demonstrated a marked reduction among the elevated-risk group individuals as opposed to those in the low-risk category (Fig. 8K).

Tumor Mutational Burden Analysis

As shown in Figures 9A and 9B, the top five most frequent genetic mutations, exhibited significant intergroup variability. TP53, PTEN, PIK3CA, ARID1A, and TTN had higher mutation rates within the elevated-risk group cohort, PTEN, PIK3CA, ARID1A, TTN, and PIK3R1 had elevated mutation rates in the low-risk cohort. Patients with low tumour mutation burden (TMB) within the elevated-risk group cohort exhibited the shortest OS (P<0.001) (Fig. 9C), with elevated tumour mutational burden correlating to extended overall survival among all UCEC patients (P<0.001) (Fig. 9D). Additionally, the elevated-risk group exhibited a marked elevation in tu-

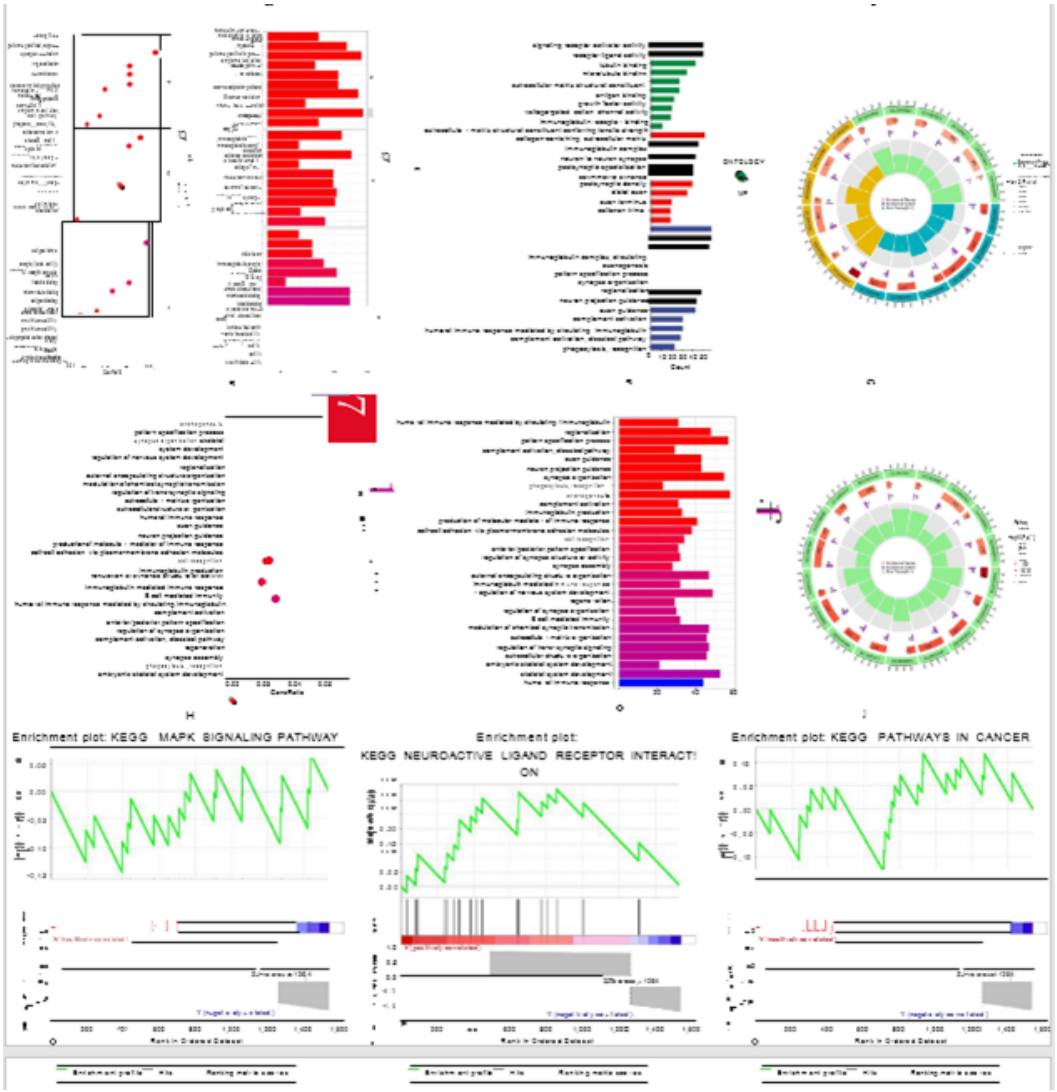

Fig. 7. GO and KEGG enrichment analysis
A-D: GO enrichment analysis
E-G: KEGG enrichment analysis
H-J: GSEA enrichment analysis

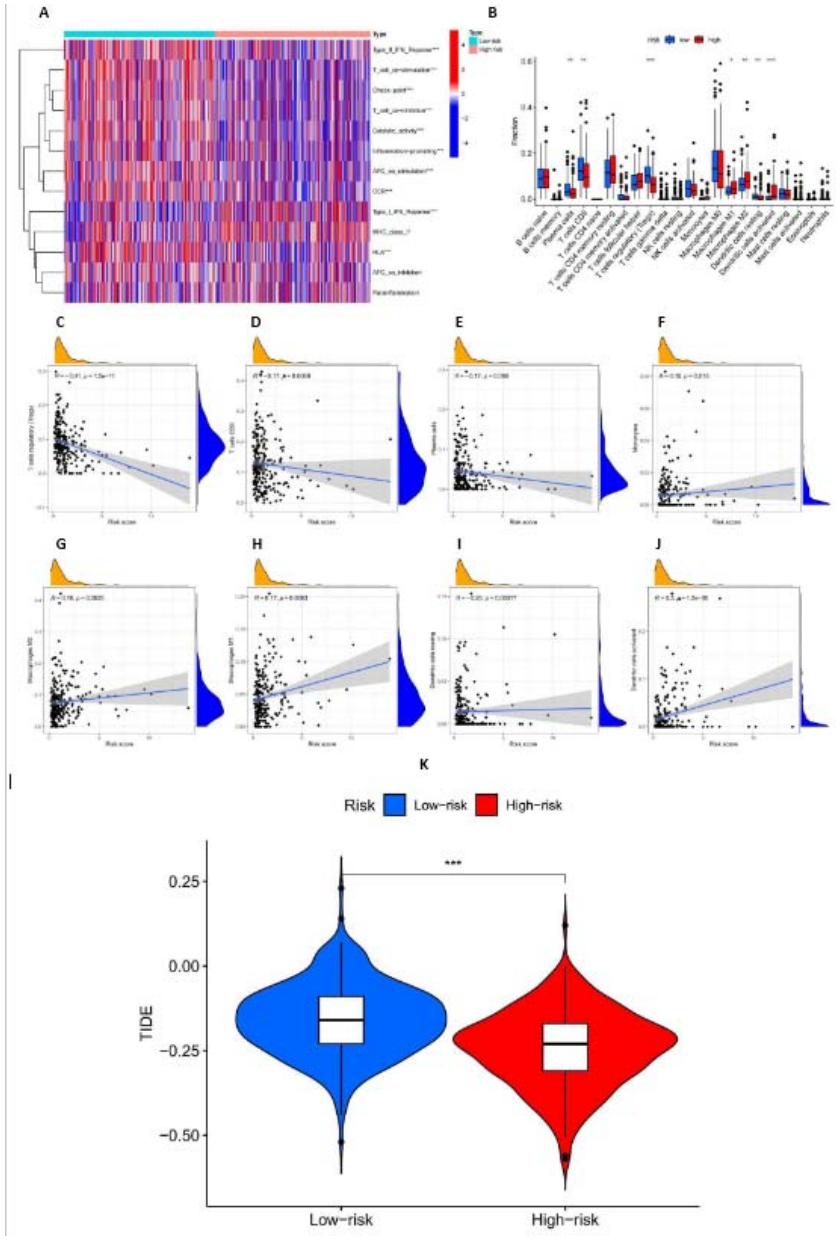

Fig. 8. Analysis of immune cell infiltration and immune escape potential
A: Differences in immune cell function between high and low risk groups
B: Difference in the proportion of immune cell infiltration between high and low risk groups
C-J: Correlation analysis of regulatory Tregs, T cells CD8, plasma cells, monocytes, macrophages M2, macrophages M1, resting dendritic cells, and activated dendritic cells infiltration in EC tissues and risk score
K: Difference analysis of tumour immune escape potential between high and low risk groups

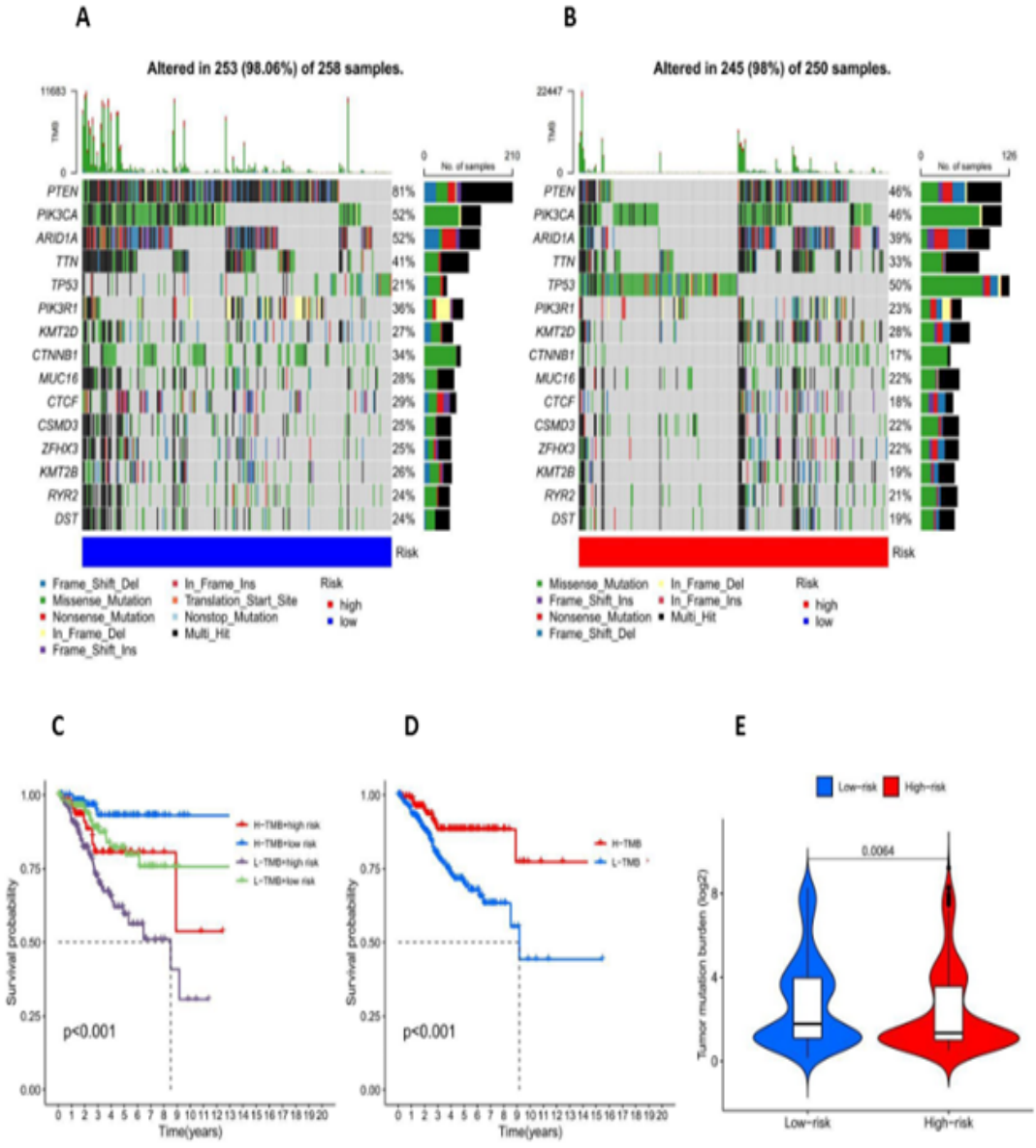

Fig. 9. Tumour mutational burden analysis
A, B: Waterfall diagram of mutant genes in low-risk and high-risk groups
C: Kaplan-Meier survival curves for OS stratified by TMB and risk score
D: Kaplan-Meier survival curve of OS stratified by TMB
E: Differences in TMB between high and low risk groups

mour mutational burden (TMB) relative versus the low-risk cohort (P=0.008) (Fig. 9E).

Antineoplastic Drug Sensitivity Prediction Using Risk Score

UCEC significant intergroup disparities differences presented among high-risk versus low-risk patient cohorts sensitivity to 75 drugs ($P<0.001$). Individuals within the elevated-risk cohort exhibited an elevated probability of being sensitive to sarubulin and phenformin, while those individuals within the low-risk cohort demonstrated an elevated propensity for respond to Bryostatin-1, BX-912, cyclospirulina, dasatinib, etoposide, bleomycin, ecoteron B, rullotinib, saratinib, sunitinib, lipoic acid, tipifarnib, and other 73 drugs (Fig. 10).

DISCUSSION

According to an investigation by Liu et al. (2022) ten disulfide-related genes, involving glycogen synthase 1 (GYS1), leucine-rich pentatricopeptide repeat-containing protein (LRPPRC), NCK-associated protein 1 (NCKAP1), NADH dehydrogenase (ubiquinone) Fe-S protein 11 (NDUFA11), NADH dehydrogenase (ubiquinone) Fe-S protein 1 (NDUFS1), nucleotide-binding protein-like (NUBPL), 3-oxoacyl-[acyl-carrier-protein] synthase (OXSM), ribophorin I (RPN1), solute carrier family 3 member 2 (SLC3A2), and solute carrier family 7 member 11 (SLC7A11), are linked to the process of disulfide stress-induced cell death. The present study found that six of these genetic loci including GYS1 (glycogen synthase), NCKAP1 (cytoskeletal regulator), NDUFA11 (mitochondrial complex I subunit), NUBPL (iron-sulfur cluster assembly factor), OXSM (fatty acid synthase component), and RPN1 (proteasome-associated protein), showed significant differences in expression between UCEC samples and normal tissues. KM curves indicated that abnormal expression of LRPPRC, NDUFA11 and OXSM in the TCGA-UCEC dataset was associated with OS.

GYS1 encodes glycogen synthase, an enzyme crucial for glycogen synthesis in the liver and muscle (Gotoh et al. 2022). Xiaoguang Liu et al. (2023) identified GYS1 and various genes involved in mitochondrial electron transport chain (NDUFS1, NDUFA11, NUBPL, and LRPPRC) as top synergistic genetic factors, whose inactivation synergistically induces cell death with glucose starvation. Another study found that treatment with endometrial bleeding-associated factor LEFTY2 markedly upregulated GYS1 mRNA expression and protein abundance in UCEC cell lines Ishikawa and HUCEC1a. In Ishikawa cells, both glucose uptake and glycogen levels exhibited notable elevations, effects not observed in benign human endometrial cells (Zeng et al. 2020). In the current study, GYS1 was upregulated in UCEC but not related to OS. The researchers speculate that high GYS1 expression in UCEC may promote glycogen content upregulation, inhibiting disulfideptosis and potentially serving as a critical driver in endometrial carcinoma pathogenesis. The NCKAP1 gene encodes a protein implicated in the reorganisation of the cytoskeleton and cellular locomotion, with varying prognostic implications in different cancers. High NCKAP1 expression shows a correlation with unfavourable outcomes in colon malignant neoplasm (Kwon et al. 2023) and breast cancer, where it stabilises the WASF3 complex, promoting metastasis (Teng et al. 2016). Conversely, in HCC, NCKAP1 improves prognosis by enhancing Rb1/p53 activation and functions as an inhibited predictive biomarker in clear cell renal carcinoma (Chen et al. 2022a; Zhong et al. 2019). The study found NCKAP1 downregulated in UCEC but not related to OS. According to Xiaoguang Liu et al. (2023), NCKAP1 loss reduced protein levels of other WRC components in SLC7A11 high-expressing cells, inhibiting disulfideptosis. The researchers speculate that low NCKAP1 expression in UCEC may disrupt WRC, inhibiting disulfideptosis in UCEC cells. The NDUFA11 gene, encoding a mitochondrial complex I subunit, is associated with various cancers. Down-regulation of NDUFA11 is linked to breast cancer (Lin et al. 2022). The current study found NDUFA11 upregulated in UCEC and associated with poor OS prognosis. LRPPRC is a multifunctional gene involved in mRNA translation and mitochondrial energy metabolism (Cui et al. 2019). Studies have shown that LRPPRC knockdown reduces apoptosis resistance, invasion, and colony development in lung adenocarcinoma and Hodgkin lymphoma cells (Tian et

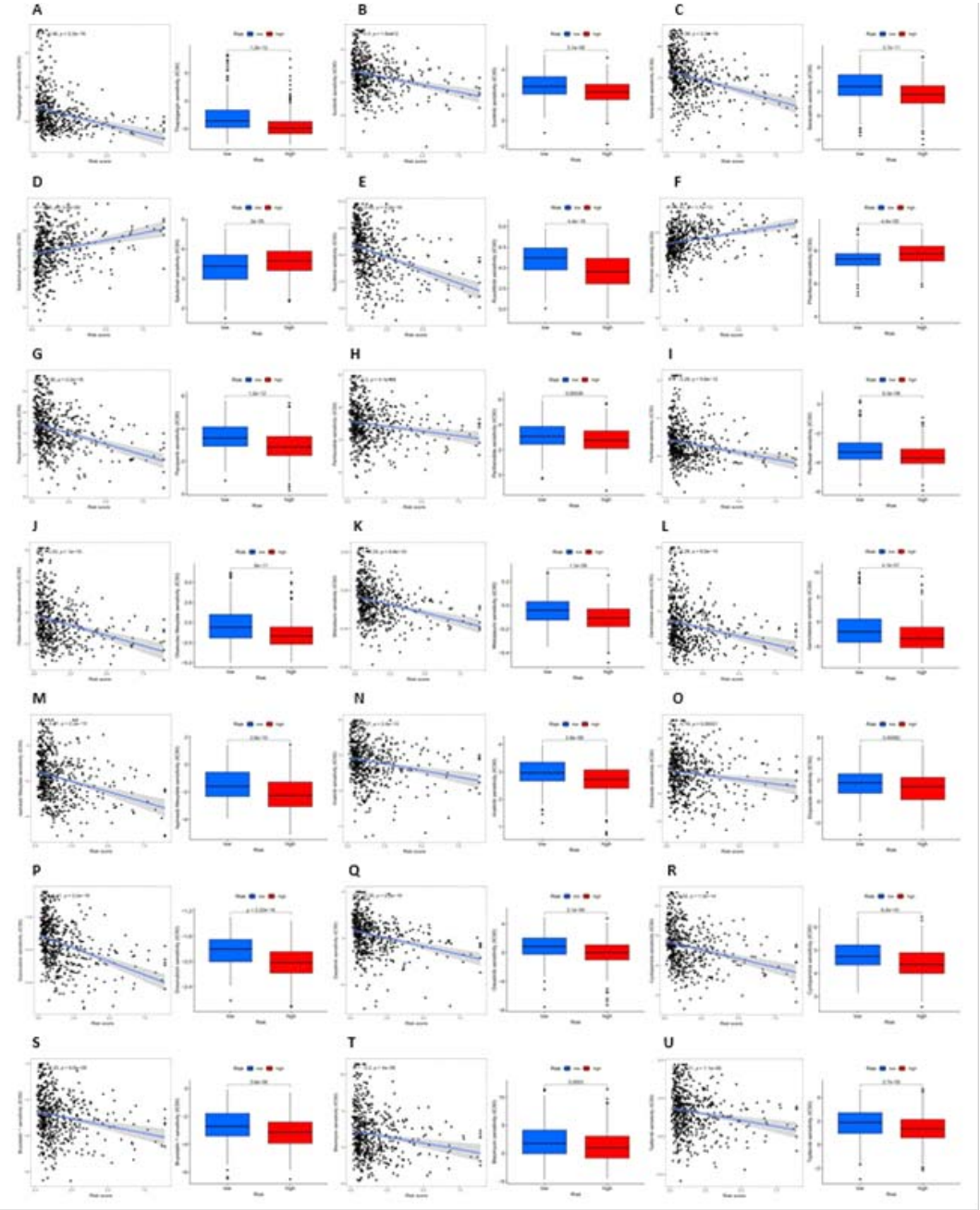

Fig. 10. Prediction of sensitivity of risk score to chemotherapy drugs by IC50 value

al. 2012), and facilitates programmed cell death in androgen-insensitive prostate carcinoma cells (Zhang et al. 2019). High LRPPRC expression is linked to poor prognosis in UCEC (Miao et al. 2021). The study confirmed where elevated LRPPRC expression correlates with unfavourable overall survival in UCEC, though no significant difference was observed between UCEC and normal tissues. NUBPL was found to be lowly expressed in UCEC, with no relation to OS. Yuhui Wang et al. (2017) identified NUBPL as a gene implicated in metastasis promoting colon cancer cell metastasis via epithelial-mesenchymal transition. OXSM, encoding a β-ketoacyl synthase, plays a role in mitochondrial fatty acid elongation. High OXSM expression is associated with poor prognosis in oral squamous cell carcinoma (Zhang et al. 2022). The investigation revealed elevated OXSM expression in UCEC, correlating with poor OS prognosis. RPN1, within the oligosaccharyltransferase (OST) complex, serves critically pertaining to N-glycan biosynthesis. Jiajun Ding et al. (2021) found RPN1 amplified in breast carcinoma, with elevated expression linked to poorer prognosis. RPN1 knockdown curtailed the growth and infiltration of mammary carcinoma cells while promoting programmed cell death through ER stress. This investigation found RPN1 highly expressed in UCEC, though not significantly correlated with OS prognosis.

The researchers used 544 TCGA database samples containing comprehensive clinical data coupled with transcriptomic sequencing information to evaluate and determine the levels of disulfideptosis-associated lncRNAs within UCEC patients and forecast OS. Via the utilisation of LASSO coupled with multivariable survival analysis analyses, the researchers identified four disulfideptosis-associated lncRNAs, developing a predictive model using their characteristics. Based on risk scores, subjects were categorised as minimal-risk and elevated-risk cohorts, and Kaplan-Meier estimates showed significantly shorter OS for the elevated-risk cohort. ROC curve analysis demonstrated the model's accuracy, validated on test and entire sets, suggesting the prognostic index serves as a standalone prognostic factor for overall survival (OS). A comprehensive diagnostic model including risk score, age, and pathological grade performed well in predicting OS, with calibration curves showing good agreement between actual and predicted OS times. The researchers' disulfideptosis-related lncRNA (drlncRNA) signature includes RAC139795.2, Z69733.1, AC020765.2, and EMSLR. AC020765.2, an autophagy-related lncRNA, acts as a protective element in non-small cell lung carcinoma (Hu et al. 2022). EMSLR, an oncogenic lncRNA, mediates aggressive cancer phenotypes and affects cell cycle progression (Hegre et al. 2021; Priyanka et al. 2022). EMSLR expression demonstrates a correlation with unfavourable outcomes in muscle-invasive bladder cancer and UCEC (Jiang et al. 2022; Zhou et al. 2022). The findings support the tumour-suppressive role of AC020765.2 and the promoting role of EMSLR in UCEC. For the other two lncRNAs, no relevant tumour research exists, providing new perspectives for further improving OS prediction in UCEC and exploring disulfideptosis-UCEC mechanisms.

The tumour microenvironment (TME) significantly impacts cancer progression (Quail and Joyce 2013; Wood et al. 2014), comprising host and cancer cell components (Anderson and Simon 2020; Baghban et al. 2020). Using the R packages GSVA and GSEAbase, the researchers assessed immune cell infiltration disparities between high- and low-risk groups and investigated the association between risk score and immune function. High-risk group patients demonstrated elevated infiltration rates of M1 and M2 macrophages alongside activated dendritic cells, whereas plasma cells, CD8+ cytotoxic T lymphocytes (CTLs), Tregs, and dormant dendritic cells exhibited elevated infiltration levels within the low-risk cohort. High-risk patients had higher immune function escape potential. Tumour-associated macrophages (TAMs) serve as key TME components (Anderson and Simon 2020; Hao et al. 2012; Sun 2016). In UCEC tissue, M1 macrophages provide pro-inflammatory responses, while M2 macrophages support the tumour immunosuppressive microenvironment (Dilara Fatma and Özkan 2023; Doran et al. 2020; Pantano et al. 2013; Zhou et al. 2020). Tregs and dendritic cells (DCs) in the TME inhibit each other (Sakaguchi et al. 2020; Wang et al. 2020; Yang et al. 2017). Higher CD8+ T cell infiltration is an independent predictor of improved OS (Jiménez-Sánchez et al. 2023). The results sug-

gest potential mechanisms activating DCs and inhibiting Tregs in high-risk patients, reducing tumour immune escape potential, and implying that immunotherapy may yield greater efficacy in high-risk patient cohorts. Significant genetic mutation discrepancies existed among the two groups, with low TMB in high-risk patients associated with shorter OS. TP53 and PTEN had the highest mutation rates in the high-risk cohort and low-risk subsets, respectively. TP53 represents an extensively researched tumour suppressor crucial for genome stability (Balaburski et al. 2010; Bernard et al. 2020; Dong et al. 2017; Sabapathy and Lane 2018; Sasaki et al. 2023). PTEN regulates metabolic processes to maintain cellular homeostasis (Chen et al. 2018; Lacroix et al. 2020; Trotman and Pandolfi 2003), with PTEN mutations linked to better survival and TP53 mutations to poor survival in UCEC (Srivastava and Vinod 2023). The study showed the best OS prognosis in high-TMB individuals classified as low-risk, aligning with previous research. The elevated tumour mutational burden among high-risk individuals supports using the risk model for individualised UCEC treatment.

There were also certain constraints within the study. The drlncRNA prognostic model was solely developed and verified utilising the TCGA dataset, requiring further independent verification. Secondary evaluation of openly accessible datasets may introduce sampling prejudice. Disulfideptosis is newly defined, needing more research to explore related genes, pathways, and mechanisms. Experimental validation is necessary to investigate drlncRNA regulation in EC progression and invasion.

In conclusion, the study identified prognostic indicators derived from risk score factor, revealing substantial variations in tumour-infiltrating lymphocyte patterns and mutational burden across risk strata. These results offer novel perspectives on disulfideptosis's function in UCEC and offer new avenues for personalised therapeutic approaches.

CONCLUSION

This study identified a predictive framework integrating four disulfideptosis-associated long noncoding RNAs that effectively predicts prognostic outcomes in patients with endometrial carcinoma of the uterine corpus (UCEC). High-risk patients classified by the model showed shorter survival, higher tumour mutation burden, and distinct immune cell infiltration patterns, including increased macrophage and dendritic cell infiltration. The model, combined with clinical features, enhances prognostic accuracy and provides insights into disulfideptosis-related mechanisms in UCEC.

RECOMMENDATIONS

Future studies should validate this prognostic model using external cohorts to confirm its generalisability. Experimental investigations are needed to clarify the functional roles of the four drlncRNAs in disulfideptosis and UCEC progression. Additionally, exploring targeted therapies based on the identified immune microenvironment differences could improve personalised treatment for UCEC patients.

CONFLICT OF INTEREST

The authors declare that the research was conducted in the absence of any commercial or financial relationships that could be construed as a potential conflict of interest.

AUTHOR CONTRIBUTIONS

Jindong Miao and Chaoqin Yu, Danying Zhang designed the research. Jindong Miao, Mengcheng Cai, Wen Cheng and Kaili Wang performed this study. Jindong Miao and Mengcheng Cai analysed the data. Jindong Miao, Mengcheng Cai and Kaili Wang wrote the paper. Chaoqin Yu, Danying Zhang, Ruipin Yao and Kaili Wang were responsible for the critical revision of the paper. Jindong Miao and Kaili Wang contributed equally to this work. All authors read and approved the final manuscript.

FUNDING

This work was funded by Shanghai Famous Traditional Chinese Medicine Academic Experience Research Studio (SHGZS-202240), Shanghai Science and Technology Commission's "Science and Technology Innovation Action Plan" Medical Innovation Research Project (20Z21900405), and The First Affiliated Hospital of Naval Medical Uni-

versity "234 Discipline Climbing Plan" (2020Y XK007).

ACKNOWLEDGMENTS

The authors sincerely thank TCGA, HPA and TIDE databases for the access of the data, and the First Affiliated Hospital of Naval Medical University for support.

DATA AVAILABILITY

The simulation experiment data used to support the findings of this study are available from the corresponding author upon request.

REFERENCES

Alhaj-Suliman SO, Naguib YW, Wafa EI, Saha S et al. 2023. A ciprofloxacin derivative with four mechanisms of action overcomes paclitaxel resistance in p53-mutant and MDR1 gene-expressing type II human endometrial cancer. *Biomaterials,* 296: 122093.

Anderson NM, Simon MC 2020. The tumor microenvironment. *Current Biology: CB,* 30: R921-r925.

Baghban R, Roshangar L, Jahanban-Esfahlan R, Seidi K et al. 2020. Tumor microenvironment complexity and therapeutic implications at a glance. *Cell Communication and Signaling: CCS,* 18: 59.

Balaburski GM, Hontz RD, Murphy ME 2010. p53 and ARF: Unexpected players in autophagy. *Trends In Cell Biology,* 20: 363-369.

Bernard E, Nannya Y, Hasserjian RP, Devlin SM et al. 2020. Implications of TP53 allelic state for genome stability, clinical presentation and outcomes in myelodysplastic syndromes. *Nature Medicine,* 26: 1549-1556.

Chen CY, Chen J, He L, Stiles BL 2018. PTEN: Tumor suppressor and metabolic regulator. *Frontiers in Endocrinology,* 9: 338.

Chen J, Ge J, Zhang W, Xie X, Zhong X, Tang S 2022a. NCKAP1 is a prognostic biomarker for inhibition of cell growth in clear cell renal cell carcinoma. *Frontiers in Genetics,* 13: 764957.

Chen J, Wang G, Luo X, Zhang J, Zhang Y 2022b. Cuproptosis patterns and tumor microenvironment in endometrial cancer. *Frontiers in Genetics,* 13: 1001374.

Cui J, Wang L, Ren X, Zhang Y, Zhang H 2019. LRPPRC: A multifunctional protein involved in energy metabolism and human disease. *Frontiers in Physiology,* 10: 595.

Dilara Fatma A, Özkan D 2023. Molecular profiling of TAM tyrosine kinase receptors and ligands in endometrial carcinoma: An in silico-study. *Taiwanese Journal of Obstetrics & Gynecology,* 62: 311-324.

Ding J, Xu J, Deng Q, Ma W, Zhang R, He X, Liu S, Zhang L 2021. Knockdown of Oligosaccharyltransferase subunit Ribophorin 1 induces endoplasmic-reticulum-stress-dependent cell apoptosis in breast cancer. *Frontiers in Oncology,* 11: 722624.

Dong ZY, Zhong WZ, Zhang XC, Su J, Xie Z, Liu SY et al. 2017. Potential predictive value of TP53 and KRAS mutation status for response to PD-1 blockade immunotherapy in lung adenocarcinoma. *Clinical Cancer Research: An Official Journal of the American Association for Cancer Research,* 23: 3012-3024.

Doran AC, Yurdagul A Jr., Tabas I 2020. Efferocytosis in health and disease. *Nature Reviews Immunology,* 20: 254-267.

Gordhandas S, Zammarrelli WA, Rios-Doria EV, Green AK, Makker V 2023. Current evidence-based systemic therapy for advanced and recurrent endometrial cancer. *Journal of the National Comprehensive Cancer Network : JNCCN,* 21: 217-226.

Gotoh H, Chimhanda TA, Nomura T, Ono K 2022. STAT3 transcriptionally regulates the expression of genes related to glycogen metabolism in developing motor neurons. *FEBS Letters,* 596: 2940-2951.

Hao NB, Lü MH, Fan YH, Cao YL, Zhang ZR, Yang SM 2012. Macrophages in tumor microenvironments and the progression of tumors. *Clinical & Developmental Immunology,* 2012: 948098.

Hecking T, Thiesler T, Halbe J, Otten L, Recker F et al. 2022. Programmed Cell Death Ligand-1 (PDL-1) correlates with tumor infiltration by immune cells and represents a promising target for immunotherapy in endometrial cancer. *Anticancer Research,* 42: 1367-1376.

Hegre SA, Samdal H, Klima A, Stovner EB, Nørsett KG et al. 2021. Joint changes in RNA, RNA polymerase II, and promoter activity through the cell cycle identify non-coding RNAs involved in proliferation. *Scientific Reports,* 11: 18952.

Hu J, Zhang PJ, Zhang D, Chen ZH, Cao XC, Yu Y, Ge J 2022. An autophagy-associated lncRNAs model for predicting the survival in non-small cell lung cancer patients. *Frontiers in Genetics,* 13: 919857.

Jiang K, Wu L, Yin X, Tang Q, Yin J, Zhou Z, Yu H, Yan S 2022. Prognostic implications of necroptosis-related long noncoding RNA signatures in muscle-invasive bladder cancer. *Frontiers in Genetics,* 13: 1036098.

Jiménez-Sánchez D, López-Janeiro Á, Villalba-Esparza M, Ariz M, Kadioglu E et al. 2023. Weakly supervised deep learning to predict recurrence in low-grade endometrial cancer from multiplexed immunofluorescence images. *NPJ Digital Medicine,* 6: 48.

Karpel HC, Slomovitz B, Coleman RL, Pothuri B 2023. Treatment options for molecular subtypes of endometrial cancer in 2023. *Current Opinion in Obstetrics & Gynecology,* 35: 270-278.

Koskas M, Amant F, Mirza MR, Creutzberg CL 2021. Cancer of the corpus uteri: 2021 update. *International Journal of Gynaecology and Obstetrics: The Official Organ of the International Federation of Gynaecology and Obstetrics,* 155(Suppl 1): 45-60.

Kulkarni U, Nayak V, Prabhu MM, Rao R 2020. Tamoxifen-induced vasculitis. *Journal of Oncology Pharmacy Practice: Official Publication of the International Society of Oncology Pharmacy Practitioners,* 26: 735-737.

Kwon MR, Lee JH, Park J, Park SS, Ju EJ et al. 2023. NCK-associated protein 1 regulates metastasis and is a novel prognostic marker for colorectal cancer. *Cell Death Discovery,* 9: 7.

Lacroix M, Riscal R, Arena G, Linares LK, Le Cam L 2020. Metabolic functions of the tumor suppressor p53: Im-

plications in normal physiology, metabolic disorders, and cancer. *Molecular Metabolism,* 33: 2-22.
Lin Y, Fan L, Zhang R, Pan H, Li Y 2022. ARSD is responsible for carcinoma and amyloidosis of breast epithelial cells. *European Journal of Cell Biology,* 101: 151199.
Lin Z, Fan W, Sui X, Wang J, Zhao J 2023. Necroptosis-related LncRNA signatures for prognostic prediction in uterine corpora endometrial cancer. *Reproductive Sciences (Thousand Oaks, Calif),* 30: 576-589.
Liu S, Zeng C, Lv H, Zhang Y, Xiong H, Tang H 2022. A novel defined pyroptosis-related gene signature for predicting the prognosis of endometrial cancer. *Disease Markers*, 2022: 7570494.
Liu X, Nie L, Zhang Y, Yan Y, Wang C, Colic M et al. 2023. Actin cytoskeleton vulnerability to disulfide stress mediates disulfidptosis. *Nature Cell Biology,* 25: 404-414.
Miao C, Fang X, Chen Y, Zhao Y, Guo Q 2021. Identification of an eight-m6A RNA methylation regulator prognostic signature of uterine corpus endometrial carcinoma based on bioinformatics analysis. *Medicine,* 100: e27689.
Murray NP, Orrego S, López MA, Munoz L, Minzer S 2019. Common B-cell acute lymphoblastic leukaemia in a 70-year-old woman presenting 2 years after carboplatin-taxane radiotherapy for endometrial cancer. *Ecancermedicalscience*, 13: 972.
Mutlu L, Harold J, Tymon-Rosario J, Santin AD 2022. Immune checkpoint inhibitors for recurrent endometrial cancer. *Expert Review of Anticancer Therapy,* 22: 249-258.
Pantano F, Berti P, Guida FM, Perrone G, Vincenzi B et al. 2013. The role of macrophages polarization in predicting prognosis of radically resected gastric cancer patients. *Journal of Cellular and Molecular Medicine,* 17: 1415-1421.
Patel JM, Enich M, Stephenson R, Groinsberg R, Girda E 2021. Vaginal mucositis related to immunotherapy in endometrial cancer. *Gynecologic Oncology Reports,* 36: 100742.
Priyanka P, Sharma M, Das S, Saxena S 2022. E2F1-induced lncRNA, EMSLR regulates lncRNA LncPRESS1. *Scientific Reports,* 12: 2548.
Qin A, Qian Q, Cui X, Bai W 2023. Ferroptosis-related lncRNA model based on CFAP58-DT for predicting prognosis and immunocytes infiltration in endometrial cancer. *Annals of Translational Medicine,* 11: 151.
Quail DF, Joyce JA 2013. Microenvironmental regulation of tumor progression and metastasis. *Nature Medicine,* 19: 1423-1437.
Sabapathy K, Lane DP 2018. Therapeutic targeting of p53: All mutants are equal, but some mutants are more equal than others. Nature reviews. *Clinical Oncology,* 15: 13-30.
Sakaguchi S, Mikami N, Wing JB, Tanaka A, Ichiyama K, Ohkura N 2020. Regulatory T cells and human disease. *Annual Review of Immunology,* 38: 541-566.
Sasaki K, Takahashi S, Ouchi K, Otsuki Y, Wakayama S, Ishioka C 2023. Different impacts of TP53 mutations on cell cycle-related gene expression among cancer types. *Scientific Reports,* 13: 4868.
Siegel RL, Miller KD, Fuchs HE, Jemal A 2022. Cancer statistics, 2022. *CA: A Cancer Journal for Clinicians,* 72: 7-33.
Srivastava A, Vinod PK 2023. Identification and characterization of metabolic subtypes of endometrial cancer using a systems-level approach. *Metabolites,* 13.
Sun Y 2016. Tumor microenvironment and cancer therapy resistance. *Cancer Letters,* 380: 205-215.
Teng Y, Qin H, Bahassan A, Bendzunas NG, Kennedy EJ, Cowell JK 2016. The WASF3-NCKAP1-CYFIP1 complex is essential for breast cancer metastasis. *Cancer Research,* 76: 5133-5142.
Tian T, Ikeda J, Wang Y, Mamat S, Luo W, Aozasa K, Morii E 2012. Role of leucine-rich pentatricopeptide repeat motif-containing protein (LRPPRC) for anti-apoptosis and tumourigenesis in cancers. *European Journal of Cancer* (Oxford, England: 1990), 48: 2462-2473.
Trotman LC, Pandolfi PP 2003. PTEN and p53: Who will get the upper hand? *Cancer Cell,* 3: 97-99.
Wang PH, Yang ST, Liu CH, Chang WH, Lee FK, Lee WL 2022. Endometrial cancer: Part I. Basic concept. *Taiwanese Journal of Obstetrics & Gynecology,* 61: 951-959.
Wang Y, Wu N, Sun D, Sun H, Tong D, Liu D et al. 2017. NUBPL, a novel metastasis-related gene, promotes colorectal carcinoma cell motility by inducing epithelial-mesenchymal transition. *Cancer Science,* 108: 1169-1176.
Wang Y, Xiang Y, Xin VW, Wang XW, Peng XC et al. 2020. Dendritic cell biology and its role in tumor immunotherapy. *Journal of Hematology & Oncology,* 13: 107.
Wood SL, Pernemalm M, Crosbie PA, Whetton AD 2014. The role of the tumor-microenvironment in lung cancer-metastasis and its relationship to potential therapeutic targets. *Cancer Treatment Reviews,* 40: 558-566.
Yang K, Blanco DB, Neale G, Vogel P, Avila J, Clish CB, Wu C et al. 2017. Homeostatic control of metabolic and functional fitness of T(reg) cells by LKB1 signalling. Nature, 548: 602-606.
Zeng N, Okumura T, Alauddin M, Khozooei S, Rajaxavier J et al. 2020. LEFTY2/endometrial bleeding-associated factor up-regulates Na+ coupled glucose transporter SGLT1 expression and glycogen accumulation in endometrial cancer cells. *PloS One,* 15: e0230044.
Zhang H, Xiao K, Zhao G, Li H, Cui J 2019. Knock-down of leucine-rich pentatricopeptide repeat containing (LRPPRC) promotes apoptosis of hormone resistant prostate cancer cells. *Xi bao yu fen zi mian yi xue za zhi = Chinese Journal of Cellular and Molecular Immunology,* 35: 419-424.
Zhang L, Zhao S, Liu Y, Lv F, Geng X 2022. Identification and validation of transcription factor-driven enhancers of genes related to lipid metabolism in metastatic oral squamous cell carcinomas. *BMC Oral Health,* 22: 126.
Zhong XP, Kan A, Ling YH, Lu LH, Mei J et al. 2019. NCKAP1 improves patient outcome and inhibits cell growth by enhancing Rb1/p53 activation in hepatocellular carcinoma. *Cell Death & Disease,* 10: 369.
Zhou XY, Dai HY, Zhang H, Zhu JL, Hu H 2022. Ferroptosis-related lncRNA for the establishment of novel prognostic signature and therapeutic response prediction to endometrial carcinoma. *Biomed Research International,* 2022: 2056913.
Zhou Y, Yao Y, Deng Y, Shao A 2020. Regulation of efferocytosis as a novel cancer therapy. *Cell Communication and Signaling: CCS,* 18: 71.

Paper received for publication in April, 2025
Paper accepted for publication in August, 2025